Vacancy multiplication following Ni L-shell photoionization

Scott B. Whitfield and G. Bradley Armen
Department of Physics and Chemical Physics Institute, University of Oregon, Eugene, Oregon 97403

Roger Carr
Stanford Synchrotron Radiation Laboratory, Stanford, California 94035

Jon C. Levin* and Bernd Crasemann
Department of Physics and Chemical Physics Institute, University of Oregon, Eugene, Oregon 97403
(Received 14 August 1987)

The mechanisms that lead to states with three and four $3d$ vacancies following L-shell photoionization of metallic Ni have been investigated with synchrotron radiation. Vacancies were created in all three L subshells, in the $L_{2,3}$ subshells, and in the L_3 subshell alone, and the resultant L_3-$M_{4,5}M_{4,5}$ Auger spectrum with its satellite structure was measured and analyzed. Auger diagram and satellite energies were computed in terms of a quasiatomic screening model, semiempirical shakeup and shakeoff cross sections were employed, and branching ratios were calculated from Auger transition theory with Hartree-Fock wave functions. Four channels leading to the four-$3d$-hole final state and three channels leading to the three-hole state, including Auger cascades and shake processes, were clearly identified and their respective roles established, convincingly verifying a model proposed by Mårtensson *et al.*

I. INTRODUCTION

Atomic inner-shell vacancies are predominantly filled by fast radiationless transitions through which additional vacancies are created before x-ray emission takes place. The multiplication of inner-shell vacancies through Auger cascades, resulting in an effective population inversion,[1] is a complex process which takes place through a multiplicity of channels.[2,3] In addition to Auger and Coster-Kronig branches, these channels include significant shakeup and shakeoff processes that arise from electron-electron Coulomb correlation.[4,5]

In recent work, Mårtensson *et al.*[6] have pointed out an interesting case of vacancy multiplication which appears to be indicated by the satellite structure of the L_3-$M_{4,5}M_{4,5}$ Auger line from metallic Ni that has been photoionized by Al $K\alpha$ radiation. One satellite feature was hypothesized to be due to a three-hole final state previously observed in Cu,[6-9] which arises from the decay of an L_3 hole in the presence of a single $3d$ spectator vacancy, i.e., an $L_3M_{4,5}$-$M_{4,5}M_{4,5}M_{4,5}$ transition. A second feature, not previously seen, was conjectured to arise from the $L_3M_{4,5}M_{4,5}$-$M_{4,5}M_{4,5}M_{4,5}M_{4,5}$ decay of an L_3 hole in the presence of two $3d$-shell spectator vacancies, leading to a final state consisting of four $3d$-shell holes.

The four-hole final state can be produced through four different channels if primary ionization is accomplished with x-ray photons whose energy exceeds the L_1 binding energy of metallic Ni, as in the experiment of Ref. 6.

(i) An L_1 primary vacancy decays by the Auger cascade

$$L_1\text{-}L_2M_{4,5}\text{-}L_3M_{4,5}M_{4,5}\text{-}M_{4,5}M_{4,5}M_{4,5}M_{4,5}\ . \quad (1)$$

(ii) Initial L_1 photoionization is accompanied by $M_{4,5}$-electron shakeup or shakeoff, and the $3d$ spectator vacancy is carried along through the Auger cascade:

$$L_1M_{4,5}\text{-}L_3M_{4,5}M_{4,5}\text{-}M_{4,5}M_{4,5}M_{4,5}M_{4,5}\ . \quad (2)$$

(iii) The initial event ionizes the L_2 shell and causes $M_{4,5}$ shakeup of shakeoff; the ensuing Auger cascade is

$$L_2M_{4,5}\text{-}L_3M_{4,5}M_{4,5}\text{-}M_{4,5}M_{4,5}M_{4,5}M_{4,5}\ . \quad (3)$$

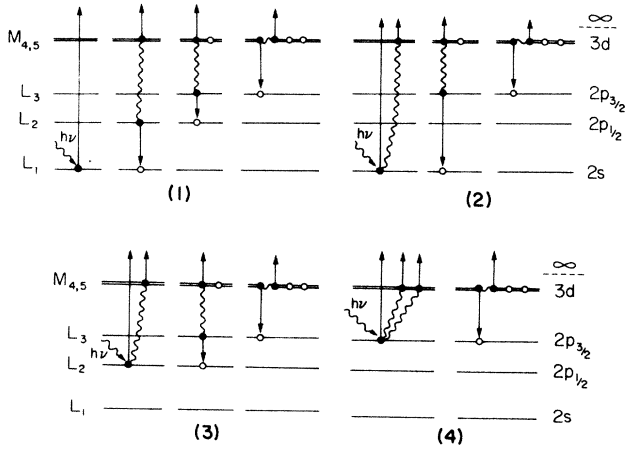

FIG. 1. Schematic representation of the four channels that lead from Ni L-shell ionization to a state with four $3d$ holes. Only active electrons and holes are shown, and direct processes are indicated, exchange transitions being omitted. Wavy lines indicate photons, real or virtual.

(iv) The initial event consists of L_3 photoionization accompanied by double $M_{4,5}$ shakeup or shakeoff; the ensuing Auger transition leads to the four-hole final state:

$$L_3M_{4,5}M_{4,5}\text{-}M_{4,5}M_{4,5}M_{4,5}M_{4,5} \ . \tag{4}$$

These channels are illustrated schematically in Fig. 1.

The three-hole final state arises through the channels

$$L_1\text{-}L_3M_{4,5}\text{-}M_{4,5}M_{4,5}M_{4,5} \ , \tag{5}$$

$$L_2\text{-}L_3M_{4,5}\text{-}M_{4,5}M_{4,5}M_{4,5} \ , \tag{6}$$

$$L_3M_{4,5}\text{-}M_{4,5}M_{4,5}M_{4,5} \ . \tag{7}$$

The mechanism leading to the four-hole state, including the relative strength of the four channels described here, can be ideally investigated with tunable synchrotron radiation. By choosing incident x rays of such energies that they can ionize all three L subshells, or only L_2 and L_3, or only L_3, it is possible to keep all four channels open, or to cut them off selectively, and to compare the resultant Auger satellite spectra. Here we describe such an experiment and its interpretation.

II. EXPERIMENT AND ANALYSIS

A. Experimental details

The measurements were performed on the JUMBO soft-x-ray line in the Stanford Synchrotron Radiation Laboratory. A narrow energy band was selected from the incident white radiation by means of a double-crystal monochromator. The $(10\bar{1}0)$ reflection from beryl crystals was used to cover the energy range from 868–1450 eV. The surface of the Ni target foil was cleaned by heating it with a current of 5 A at 2 V *in vacuo* (4×10^{-9} Torr) through the sample.

Electron spectra were measured with a commercial double-pass cylindrical mirror analyzer in the pulse-counting mode. The electron spectrometer pass energy was 100 eV. The experiment was controlled by a Digital Equipment Corporation PDP11/34 computer.

B. Kinetic energies

Measured Auger electron spectra excited with incident x rays of energies 1450, 910, and 868 eV are indicated in Fig. 2. Quantitative analysis of the intensity and kinetic energy of the satellites can be performed by invoking the screening model employed by Johansson and Mårtensson.[10,11] This model allows one to treat certain metal Auger spectra from an essentially atomic point of view, as long as the interaction energy U between holes in the conduction band equals or exceeds the bandwidth W. When the condition $U/W \geq 1$ is fulfilled, the solid-state spectrum splits into two parts:[12] a residual self-convoluted valence-band spectrum and a "quasiatomic" part. The latter can be treated as in free atoms. With $U=3.65$ eV and $W=3.8$ eV, nickel falls within the range of applicability of this model.[12]

The screening model is best illustrated by means of an example. We consider prediction of the kinetic energy

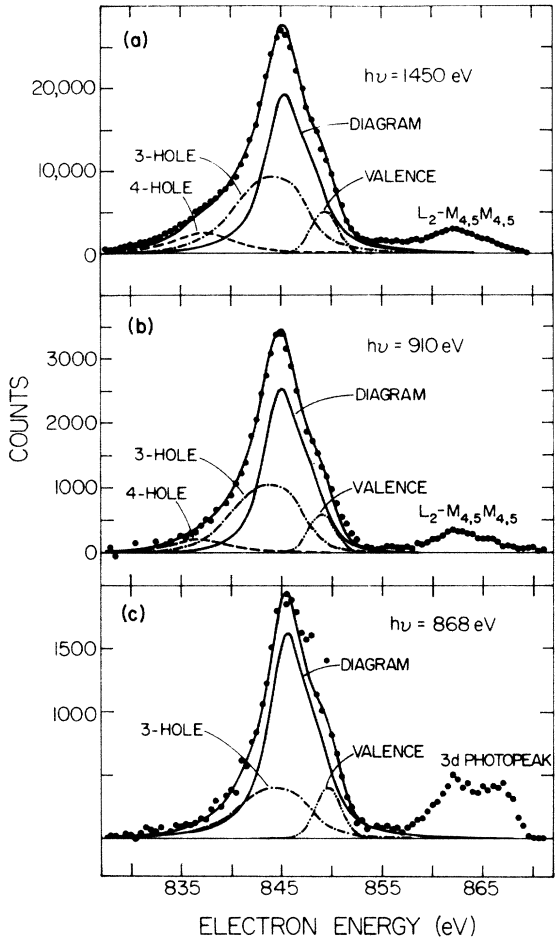

FIG. 2. Nickel L_3-$M_{4,5}M_{4,5}$ Auger electron spectra excited with synchrotron radiation of energies 1450, 910, and 868 eV, respectively, ionizing all three L subshells (a), the L_2 and L_3 subshells (b), and only the L_3 subshell. Decomposition of the spectra into diagram and satellite peaks is indicated as discussed in the text.

of the ^1G component of the diagram multiplet of the L_3-$M_{4,5}M_{4,5}$ Auger transition; this line is located at the centroid of the Ni metal L_3-$M_{4,5}M_{4,5}$ spectrum.[6,11,13,14] The starting point is the ground-state configuration of a Ni atom in the metal, $(\mathrm{Ar})\{3d^9 4s^1\}$, where the curly brackets indicate that the site in question is in a metallic state. To find the energy of the initial state prior to Auger decay we consider the following steps:

$$\begin{aligned}(\mathrm{Ar})\{3d^9 4s^1\} &\rightarrow (\mathrm{Ar})3d^8 4s^2 \rightarrow (\mathrm{Ar})3d^9 4s^1 \\ &\rightarrow (\mathrm{Ar})[2p_{3/2}]3d^{10}4s^1 \\ &\rightarrow (\mathrm{Ar})[2p_{3/2}]3d^{10}\{4s^1\} \ .\end{aligned} \tag{8}$$

(Here as in the following, square brackets indicate holes.) The first step in Eq. (8) takes an atom from its ground state in the metal to the ground state of a free atom; the energy change here is thus simply the cohesive energy of Ni. The second step leads to an excited state of the free atom which resembles the ground state of an atom in the

metal. The third step involves two processes: the removal of a $2p_{3/2}$ electron by photoionization and screening of the $2p_{3/2}$ hole by a $3d$ electron from the metal. The final step places the screened Ni atom back into its metallic state. Here the atom appears as if it were a Cu impurity atom imbedded in a Ni host, hence the energy change is approximately the cohesive energy of Cu.[11] The initial state being thus defined, its energy can be readily calculated with a standard Hartree-Fock code[15] and tabulated values of the cohesive energy.[16]

The final state is calculated through the series of steps

$$\begin{aligned}(\mathrm{Ar})[2p_{3/2}]3d^{10}\{4s^1\} &\rightarrow (\mathrm{Ar})[2p_{3/2}]3d^{10}4s^1 \\ &\rightarrow (\mathrm{Ar})3d^8 4s^2 \rightarrow (\mathrm{Ar})3d^8 4s^2(^1G) \\ &\rightarrow (\mathrm{Ar})3d^8\{4s^2(^1G)\} \ . \end{aligned} \quad (9)$$

As before, the first step involves the energy associated with taking the atom out of the metal into a free atomic state. The second step takes account of the Auger decay and the simultaneous screening of the additional hole that results from this process. It should be noted that here the screening electron is a $4s$ electron because in the presence of the $2p$ hole the $3d$ electrons are localized. The third step represents the energy difference between the configuration average and the ^1G multiplet state. The last step again places the screened Ni atom back into the metal. Here the configuration in curly brackets is identical to that found in Zn, and thus the energy change is approximately the cohesive energy of Zn.

The kinetic energy of the ^1G multiplet component in the Ni Auger spectrum is the difference between the energies of the $(\mathrm{Ar})[2p_{3/2}]3d^{10}\{4s^1\}$ initial state and the $(\mathrm{Ar})3d^8\{4s^2(^1G)\}$ final state. The results from Hartree-Fock calculations[15] with inclusion of the appropriate cohesive energies[16] for Ni, Cu, and Zn are compared in Table I with experimental values and the free-atom Hartree-Fock transition energies. There is excellent agreement with experiment, which appears to validate the use of this screening model.

Based on this example, the following formula can be used to calculate the kinetic energy E_A of the Auger electrons in the Ni L_3-$M_{4,5}M_{4,5}$ spectrum:

$$E_A = (E_i^s - C_i + X_i) - (E_f^s - C_f + X_f) \ . \quad (10)$$

Here, E_i^s and E_f^s are the configuration-average energies of the fully screened initial and final states, respectively; C_i and C_f are the corresponding cohesive energies; and X_i and X_f are the differences between the energies of the initial- and final-state multiplet components, respectively, and the corresponding configuration averages. According to this model, the initial and final configurations for the three-hole state are $(\mathrm{Ar})[2p_{3/2}]3d^9\{4s^2\}$ and $(\mathrm{Ar})3d^7\{4s^2 4p^1\}$, while for the four-hole state we have $(\mathrm{Ar})[2p_{3/2}]3d^8\{4s^2 4p^1\}$ and $(\mathrm{Ar})3d^6\{4s^2 4p^2\}$.

The energies of the multiplet components of the main line and the configuration averages of the three-hole and four-hole satellites were calculated from Eq. (10), using the Froese-Fischer Hartree-Fock code,[15] the appropriate cohesive energies,[16] and Slater's tables of Coulomb splittings[17] for the multiplets. Results are listed in Table II.

C. Satellite intensities

The intensity I of an Auger line in a measured spectrum is determined by several factors:

$$I \propto \sigma(nlj, E_x) B S(E_e) N_x(E_x, T) g \ . \quad (11)$$

Here, $\sigma(nlj, E_x)$ is the cross section for producing the initial vacancy characterized by quantum numbers nlj with x rays of energy E_x, B is the pertinent Auger branching ratio in the decay of the initial vacancy, and $S(E_e)$ is the spectrometer transmission function which depends on the kinetic energy E_e of the detected electrons. The total number of photons of energy E_x that impinge upon the sample in the course of the measurement of duration T is denoted by $N_x(E_x, T)$, and g is a geometrical factor. For the present purposes, it is sufficient to consider only the *relative* intensities of the satellites and main line. Within a single spectrum, the intensity ratio of two features 1 and 2 is

$$\frac{I_1}{I_2} = \frac{\sigma_1(nlj, E_x) B_1}{\sigma_2(n'l'j', E_x) B_2} \ . \quad (12)$$

TABLE I. Ni, Cu, and Zn L_3-$M_{4,5}M_{4,5}$ Auger-electron energies (in eV).

	Solid (^1G)		Free atom	
Element	Theory	Expt.	Theory	Expt.
Ni	845.48[a]	846.2[b]	821.26[a,c]	822[d]
Cu	917.76[a]	918.75[e]	900.85[a,f]	900.80[g]
Zn	990.00[a]	992.00[e]	972.90[a]	973.4[h]

[a]Present work.
[b]Reference 6.
[c]Configuration average.
[d]K. Aksela, S. Aksela, T. Pekkala, and M. Wallenius, Phys. Rev. A **35**, 1522 (1987).
[e]Reference 14.
[f]^2G.
[g]S. Aksela and J. Sivonen, Phys. Rev. A **25**, 1243 (1982).
[h]S. Aksela, J. Väyrynen, and H. Aksela, Phys. Rev. Lett. **33**, 999 (1974).

TABLE II. Calculated energies (in eV) of L_3-$M_{4,5}M_{4,5}$ Auger electrons and satellites in metallic Ni.

Transition	Component	Energy	Separation from L_3-$M_{4,5}M_{4,5}$ (^1G)
L_3-$M_{4,5}M_{4,5}$	^3F	848.60	3.12
	CA[a]	847.10	1.62
	^1D	846.61	1.13
	^3P	846.18	0.70
	^1G	845.48	0
	^1S	840.92	−4.56
L_3-$M_{4,5}^3$	CA	843.57	−1.91[b]
L_3-$M_{4,5}^4$	CA	837.73	−7.75[c]

[a]CA stands for configuration average.
[b]The result of Ref. 6 is −2 eV.
[c]The result of Ref. 6 is −7 eV.

Cross sections $\sigma_i(nlj,E_x)$ for photoionization were taken from the theoretical tables of Scofield;[18] for vacancy production by shakeup and shakeoff these cross sections were determined with the aid of experimental photoelectron spectra as described below. The Auger branching ratios B_i were calculated from theory, as described below, with fully screened Hartree-Fock wave functions.

We illustrate the calculation of relative intensities by deriving the intensity ratio of the four-hole satellite to the main Auger line excited with photons of sufficient energy to ionize the L_2 and L_3 subshells but not the L_1 subshell (i.e., $E_x=910$ eV in this experiment). Only the channels described by Eqs. (3) and (4) are then open, and the intensity of the Auger satellite associated with the four-hole final state is

$$I_4 \propto \sigma'(2p_{1/2})B(L_2M_{4,5}\text{-}L_3M_{4,5}^2)B(L_3M_{4,5}^2\text{-}M_{4,5}^4) + \sigma''(2p_{3/2})B(L_3M_{4,5}^2\text{-}M_{4,5}^4) , \quad (13)$$

while the main-line intensity is proportional to

$$I_2 \propto \sigma(2p_{3/2})B(L_3\text{-}M_{4,5}M_{4,5}) . \quad (14)$$

The cross section denoted by $\sigma'(2p_{1/2})$ in Eq. (13) pertains to photoionization of an L_2 electron accompanied by shakeup or shakeoff of one $M_{4,5}$ electron, and $\sigma''(2p_{3/2})$ is the cross section for photoionization of an L_3 electron accompanied by shakeup or shakeoff of two $M_{4,5}$ electrons. To evaluate the ratio of Eqs. (13) and (14) we make the approximation that the presence of one or two $M_{4,5}$ spectator vacancies does not significantly affect the Auger branching ratios, i.e.,

$$B(L_2M_{4,5}\text{-}L_3M_{4,5}^2)\cong B(L_2\text{-}L_3M_{4,5}) , \quad B(L_3M_{4,5}^2\text{-}M_{4,5}^4)\cong B(L_3\text{-}M_{4,5}M_{4,5}) . \quad (15)$$

We then have

$$\frac{I_4}{I_2}\cong\frac{\sigma'(2p_{1/2})B(L_2\text{-}L_3M_{4,5})+\sigma''(2p_{3/2})}{\sigma(2p_{3/2})} . \quad (16)$$

The cross sections σ' for L_2 and L_3 photoionization accompanied by single $3d$-electron shakeup or shakeoff were determined semiempirically by analyzing L_2 and L_3 photoelectron spectra as shown in Fig. 3. Single $M_{4,5}$-electron shakeup or shakeoff satellites are discernible some 6 eV below the main photoionization peaks. The area under each photoionization peak plus single-shake satellite was determined by numerical integration. The photoionization peaks alone exhibit a pure Voigt profile; although there is multiplet splitting in the satellites there is none in the photopeaks, due to $3d$-electron screening, since the $4s$ electron participates in the metallic bonding and thus will not couple with the nonbonding p electrons. Hence the photopeaks could be fitted with Pearson-7 functions (solid curves in Fig. 3); these four-parameter functions are continuously variable from Lorentzian to Gaussian and hence are ideally suited to model Voigt shapes. The cross-section ratio $a(2p_j)$ for photoionization accompanied by single $3d$ shakeup or shakeoff to pure photoionization was thus measured:

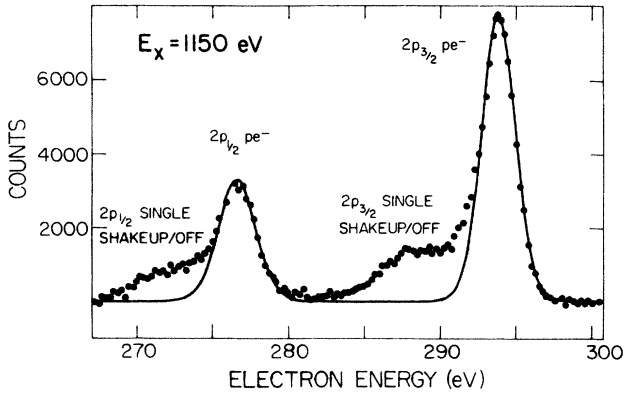

FIG. 3. Nickel $L_{2,3}$ photoelectron spectrum including shakeup and shakeoff satellites, excited with 1150-eV synchrotron radiation.

$$\sigma'(2p_j)=a(2p_j)\sigma(2p_j) , \quad (17)$$

with $\sigma(2p_j)$ taken from Scofield's tables.[18]

The double shakeup-shakeoff satellites are not sufficiently well resolved in our photoelectron spectra (Fig. 3) to determine σ''. We draw upon the experimental result of Bosch *et al.*[19] that the intensity of the Ni L_2 double-shake satellite is $\sim 2\%$ of the photoelectron line, and assume that approximately the same ratio holds for the L_3 satellite.

For the case in which all four channels indicated by Eqs. (1)–(4) are open we also require the value of $\sigma'(2s)$. The width of the L_1 photopeak prevents an experimental determination of $a(2s)$, and we approximate the result by taking $a(2s)\cong a(2p_{1/2})$. All pertinent cross-section ratios are summarized in Table III.

The relative intensities of the five diagram Auger multiplet components and the 48 multiplet components comprising the three-hole-state satellite were computed in a conventional manner[20–23] from Hartree-Fock wave functions. We consider the problem in the frozen-core approximation. The relevant transitions are $[2p]\rightarrow[3d]^2$ and $[2p3d]\rightarrow[3d]^3$ for the diagram line and the three-hole-state satellite, respectively. The initial and final states for these types of transitions are

$$|i\rangle=|l_1^m(V_mS_mL_m)l_2^n(V_nS_nL_n)SL\rangle , \quad (18)$$

$$|f\rangle=|l_1^{m+1}(V_m'S_m'L_m')l_2^{n-2}(V_n'S_n'L_n')S_1L_1l_ASL\rangle . \quad (19)$$

TABLE III. Ratios (estimated at $E_x=1150$ eV) of cross sections for $2l_j$-subshell photoionization of Ni accompanied by single and double $3d$-electron shakeup or shakeoff [$\sigma'(2lj)$ and $\sigma''(2lj)$, respectively] to pure $2l_j$ photoionization cross sections.

Ratio	Value
$\sigma'(2p_{3/2})/\sigma(2p_{3/2})$	0.42±0.04
$\sigma''(2p_{3/2})/\sigma(2p_{3/2})$	0.02±0.03[a]
$\sigma'(2p_{1/2})/\sigma(2p_{1/2})$	0.49±0.05
$\sigma'(2s)/\sigma(2s)$	0.49±0.05

[a]Reference 19.

Here, l_1 is the orbital angular momentum of an electron in the subshell that contains the initial vacancy, l_2 is the angular momentum of an electron in the subshell from which the initial vacancy is filled in a direct transition, m is the occupation number corresponding to l_1, n is the occupation number corresponding to l_2, and l_A is the orbital angular momentum of the Auger electron in its final continuum state. The m electrons of orbital angular momentum l_1 in the initial state couple to total spin S_m and total orbital angular momentum L_m with seniority number V_m. Similarly, the n electrons of angular momentum l_2 couple to total spin S_n and total orbital angular momentum L_n. These two subshells then couple to yield total spin S and total orbital angular momentum L. Analogous coupling applies for the final state. The transition intensity of a given multiplet Auger component thus is

$$I=\frac{2\pi}{\hbar}\frac{(2S_1+1)(2L_1+1)}{2(2l_1+1)}\sum_{l_A}|\langle f\,|\,1/r_{12}\,|\,i\rangle|^2\,, \tag{20}$$

where the matrix element is

$$\langle f\,|\,e^2/r_{12}\,|\,i\rangle=\sum_k a^k R^k(l_1 l_A l_2 l_2)\,. \tag{21}$$

The angular factors a^k are determined from Racah algebra and depend on the configurations of the initial and final states and the coupling scheme. For the initial and final states given by Eqs. (18) and (19), respectively, Racah algebra yields

$$a^k=(-1)^{\alpha}\sqrt{(m+1)n(n-1)}[S_n,L_n,S'_m,L'_m,l_1,l_2,l_A,l_2]^{1/2}(l_1^{m+1}V'_mS'_mL'_m\{\,|\,l_1^mV_mS_mL_m)\begin{bmatrix}l_1&k&l_2\\0&0&0\end{bmatrix}\begin{bmatrix}l_A&k&l_2\\0&0&0\end{bmatrix}$$
$$\times\sum_{\bar V_n\bar S_n\bar L_n}\Bigg[(l_2^nV_nS_nL_n\{\,|\,l_2^{n-1}\bar V_n\bar S_n\bar L_n)(l_2^{n-1}\bar V_n\bar S_n\bar L_n\{\,|\,l_2^{n-2}V'_nS'_nL'_n)[\bar S_n,\bar L_n]^{1/2}$$
$$\times\begin{Bmatrix}S_1&\frac12&S\\S_n&S_m&\bar S_n\end{Bmatrix}\begin{Bmatrix}S_1&S'_n&S'_m\\\frac12&S_m&\bar S_n\end{Bmatrix}\begin{Bmatrix}L'_m&L_m&l_1&k\\L_1&L&l_A&\bar L_n\\L'_n&L_n&l_2&l_2\end{Bmatrix}\Bigg]\,, \tag{22}$$

where $\alpha=n+L_m+L'_m+l_2+S+\frac12-S_1$. Square brackets as in $[S_i,L_i]$ have been used as abbreviation for $(2S_i+1)(2L_i+1)$, and the 12-j symbol is defined as follows:

$$\begin{Bmatrix}j_1&j_2&j_3&j_4\\j_5&j_6&j_7&j_8\\j_9&j_{10}&j_{11}&j_{12}\end{Bmatrix}=(-1)^{\beta}\sum_{i=|j_2-j_5|}^{j_2+j_5}\Bigg[(2i+1)(-)^{3i}\begin{Bmatrix}j_2&j_5&i\\j_9&j_3&j_1\end{Bmatrix}\begin{Bmatrix}j_9&j_3&i\\j_4&j_8&j_{11}\end{Bmatrix}$$
$$\times\begin{Bmatrix}j_4&j_8&i\\j_{10}&j_7&j_{12}\end{Bmatrix}\begin{Bmatrix}j_{10}&j_7&i\\j_5&j_2&j_6\end{Bmatrix}\Bigg],\quad \beta=\sum_{i=1}^{12}j_i\,. \tag{23}$$

The radial part of the matrix element is a Slater integral,[24]

$$R^k(n_1l_1n_2l_2,n_3l_3n_4l_4)=\int\int R_{n_1l_1}(r_1)R_{n_2l_2}(r_2)\frac{r_<^k}{r_>^{k+1}}R_{n_3l_3}(r_1)R_{n_4l_4}(r_2)r_1^2r_2^2dr_1dr_2\,, \tag{24}$$

where $r_<$ and $r_>$ are the lesser and the greater of r_1 and r_2, respectively. For the present work, the requisite Auger rates were computed with codes for the radial elements[23] and for the angular factors based on the above formalism.[22]

In Table IV, calculated satellite intensities are listed and compared with computed results from Ref. 6. There is satisfactory agreement, even though the authors of Ref. 6 drew upon McGuire's Auger rates[25] which do not account for screening as ours do, and used a Dirac-Fock program for the energy calculations while we have used a nonrelativistic Hartree-Fock code.

D. Comparison between calculations and experimental data

The contribution of low-energy scattered electrons from the solid-state target was removed from the measured spectra by means of an iteration routine.[26] It was assumed that this background at any energy in a spectrum is proportional, by a constant factor, to the integrated intensity encountered above that energy. The corrected data are shown in Fig. 2.

Included in Fig. 2 is the calculated decomposition of the measured spectra, broadened consistently to attain a best fit. The diagram multiplet is composed of five com-

TABLE IV. Intensities (relative to the $n=2$ diagram peak) of Ni L_3-$M^n_{4,5}$ Auger satellites from $n=3$ and $n=4$ final states, excited with incident x rays of various energies. Contributions of various channels to the formation of the $n=4$ satellite are indicated for the highest excitation energy.

X-ray energy (eV)	Channel[a]	Present work $n=3$ satellite	Present work $n=4$ satellite	Ref. 6 $n=4$ satellite
1486[b]				0.2–0.3
1450[b]		0.801±0.04	0.238±0.024	
	1		0.027[c]	~0.025
	2		0.055±0.006	~0.050
	3		0.131±0.013	~0.125
	4		0.025±0.005	~0.050
910[d]		0.710±0.04	0.167±0.020	
868[e]		0.419±0.04	0	

[a]Channels 1–4 are as described in Eqs. (1)–(4), respectively.
[b]All three L subshells are ionized.
[c]Derived from theory.
[d]The L_2 and L_3 subshells are ionized.
[e]Only the L_3 subshell is ionized.

ponents with separations as indicated in Table II. These components were modeled with Pearson-7 functions of identical shape and width.

The positions relative to the configuration average of the 48 multiplet components of the three-hole-state satellite (indicated in Table II) were calculated from Slater's[17] tables of Coulomb splittings. Relative intensities of these components were calculated from Auger-transition theory,[18–23] as described above. Because of large overlap among many of the multiplet components, the three-hole satellite feature could be modeled with a total of only 20 peaks. The shape and width of these 20 peaks were taken to be the same, and identical to those of the diagram-line components. The calculated energy separation between the three-hole satellite and the centroid of the diagram peak, which coincides with the ^1G multiplet component, is 1.91 eV (Table II). The relative intensity of the three-hole satellite with respect to the diagram peak is as indicated in Table IV.

The four-hole satellite was modeled by a single peak because its multiplet components are too numerous to consider independently. This satellite lies 7.75 eV below the diagram-peak centroid (Table II); its relative intensities at the various incident x-ray energies are as indicated in Table IV.

There is a sizable self-convoluted valence-band peak in these spectra. The shape of this peak was taken to be Gaussian, and its width and intensity were allowed to float so at to attain a best fit in the spectrum taken with 1450-eV x rays. The valence-band peak width, relative intensity, and position were then held constant for all spectra. In fitting the 27 peaks to the measured spectra, four free parameters were thus employed: the energy of the diagram-peak centroid, the intensity of the diagram peak, the width of the diagram multiplet components, and the Pearson-7 parameter that determines the shape (from Lorentzian to Gaussian) of the individual lines. These four parameters were varied to attain a best fit to the data, and kept constant for all three spectra.

III. CONCLUSIONS

As can be seen from Fig. 2, agreement between theory and experiment is excellent, with satellite intensities depending on the incident x-ray energies in complete accord with the model underlying Eqs. (1)–(4) and (5)–(7). The mechanism proposed in Ref. 6 for the formation of the multiplet satellites is thus convincingly verified. Furthermore, the agreement between calculated and measured spectra strongly supports the validity of the screening model,[10,11] indicating that these metallic Auger spectra of Ni can be understood remarkably well in terms of a quasiatomic picture.

ACKNOWLEDGMENTS

We gratefully acknowledge helpful conversations with F. P. Larkins and G. S. Brown, advice on the analysis from S. L. Sorensen, and technical assistance from Mike Rowan. This work was supported in part by National Science Foundation Grant No. PHY-8516788 and U.S. Air Force Office of Scientific Research Grant No. AFOSR-87-0026. The Stanford Synchrotron Radiation Laboratory, where the experiment was performed, is supported by the U.S. Department of Energy (through the Office of Basic Energy Sciencies) and by the National Institutes of Health (through the Biotechnology Resources Program).

*Present address: Oak Ridge National Laboratory, Oak Ridge, TN 37830.

[1]H. C. Kapteyn, R. W. Lee, and R. W. Falcone, Phys. Rev. Lett. **57**, 2939 (1986).

[2]P. Venugopala Rao, M. H. Chen, and B. Crasemann, Phys. Rev. A **5**, 997 (1972).

[3]V. L. Jacobs, L. Davis, B. F. Rozsnyai, and J. W. Cooper, Phys. Rev. A **21**, 1917 (1980).

[4]T. Åberg, Phys. Rev. **156**, 35 (1967); in *Photoionization and Other Probes of Many-Electron Interactions,* edited by F. Wuilleumier (Plenum, New York, 1976), p. 49.

[5]G. B. Armen, T. Åberg, K. R. Karim, J. C. Levin, B. Crasemann, G. S. Brown, M. H. Chen, and G. E. Ice, Phys. Rev. Lett. **54**, 182 (1985).

[6]N. Mårtensson, R. Nyholm, and B. Johansson, Phys. Rev. B **30**, 2245 (1984).

[7]N. Mårtensson and B. Johansson, Phys. Rev. B **28**, 3733 (1983).

[8]P. Weightman and P. T. Andrews, J. Phys. C **12**, 1943 (1979).

[9]H. W. Haak, G. A. Sawatzky, and T. D. Thomas, Phys. Rev. Lett. **41**, 1825 (1978).

[10]B. Johansson and N. Mårtensson, Phys. Rev. B **21**, 4427 (1980).

[11]N. Mårtensson and B. Johansson, Phys. Rev. Lett. **45**, 482 (1980).

[12]P. A. Bennett, J. C. Fuggle, F. U. Hillebrecht, A. Lenselink, and G. A. Sawatzky, Phys. Rev. B **27**, 2194 (1983).

[13]A. M. Baro, M. Salmeron, and J. M. Rojo, J. Phys. F **5**, 826 (1975).

[14]L. I Yin, I. Adler, M. H. Chen, and B. Crasemann, Phys. Rev. A **7**, 897 (1973); L. I Yin, I. Adler, T. Tsang, M. H. Chen, and B. Crasemann, Phys. Lett. **A46**, 113 (1973).

[15]C. Froese-Fischer, Comput. Phys. Commum. **8**, 329 (1974).

[16]C. Kittel, *Introduction to Solid State Physics,* 3rd ed. (Wiley, New York, 1966).

[17]J. C. Slater, *Quantum Theory of Atomic Structure* (McGraw-Hill, New York, 1960), Vol. I.

[18]J. H. Scofield, Lawrence Livermore National Laboratory Report No. UCRL-51326, 1973 (unpublished).

[19]A. Bosch, H. Feil, G. A. Sawatzky, and N. Mårtensson, Solid State Commun. **41**, 355 (1982).

[20]M. H. Chen, in *Atomic Inner-Shell Physics,* edited by B. Crasemann (Plenum, New York, 1985), Chap. 2.

[21]V. O. Kostroun, M. H. Chen, and B. Crasemann, Phys. Rev. A **3**, 533 (1971).

[22]M. H. Chen, Phys. Rev. A **31**, 1449 (1985).

[23]G. B. Armen, Ph.D. thesis, University of Oregon, 1985.

[24]M. Aoyagi, M. H. Chen, B. Crasemann, K.-N. Huang, and H. Mark, NASA Technical Report No. NASA TR R-464, 1977.

[25]E. J. McGuire, Phys. Rev. A **3**, 1801 (1971).

[26]E. Antonides, E. C. Janse, and G. A. Sawatzky, Phys. Rev. B **15**, 1669 (1977).